PNAS RESEARCH ARTICLE | MEDICAL SCIENCES OPEN ACCESS

Mosaic RBD nanoparticles induce intergenus cross-reactive antibodies and protect against SARS-CoV-2 challenge

Dan Bi Lee[a,1], Hyojin Kim[b,1], Ju Hwan Jeong[c,1], Ui Soon Jang[a,d], Yuyeon Jang[a,d], Seokbeom Roh[a,d], Hyunbum Jeon[e], Eun Jeong Kim[a], Su Yeon Han[a], Jin Young Maeng[b], Stefan Magez[f,g,h], Magdalena Radwanska[f,i], Ji Young Mun[j], Hyun Sik Jun[a,d], Gyudo Lee[a,d], Min-Suk Song[c], Hye-Ra Lee[a,d], Mi Sook Chung[b,2], Yun Hee Baek[c,2], and Kyung Hyun Kim[a,2]

Edited by Pamela Bjorkman, California Institute of Technology, Pasadena, CA; received May 19, 2022; accepted November 29, 2022

Recurrent spillovers of α- and β-coronaviruses (CoV) such as severe acute respiratory syndrome (SARS)-CoV, Middle East respiratory syndrome-CoV, SARS-CoV-2, and possibly human CoV have caused serious morbidity and mortality worldwide. In this study, six receptor-binding domains (RBDs) derived from α- and β-CoV that are considered to have originated from animals and cross-infected humans were linked to a heterotrimeric scaffold, proliferating cell nuclear antigen (PCNA) subunits, PCNA1, PCNA2, and PCNA3. They assemble to create a stable mosaic multivalent nanoparticle, 6RBD-np, displaying a ring-shaped disk with six protruding antigens, like jewels in a crown. Prime-boost immunizations with 6RBD-np in mice induced significantly high Ab titers against RBD antigens derived from α- and β-CoV and increased interferon (IFN-γ) production, with full protection against the SARS-CoV-2 wild type and Delta challenges. The mosaic 6RBD-np has the potential to induce intergenus cross-reactivity and to be developed as a pan-CoV vaccine against future CoV spillovers.

SARS-CoV-2 | spike | receptor-binding domain | mosaic multivalent antigens | immune response

The incidence of emerging infectious diseases has increased in the past 80 y (1), which is considered to be caused primarily by a zoonotic spillover, posing ongoing human health threats (2, 3). Recurrent spillovers of α- and β-coronaviruses (CoV), including severe acute respiratory syndrome (SARS)-CoV, Middle East respiratory syndrome (MERS)-CoV, SARS-CoV-2, and possibly human CoV (hCoV), have caused serious morbidity and mortality worldwide (4).

Active SARS-CoV-2 spike glycoproteins, comprising two subunits S1 and S2, play a key role in receptor binding and membrane fusion for cell entry, leading to the primary target of neutralizing antibodies (nAbs) (5). The S1 subunit consists of an N-terminal domain (NTD), a receptor-binding domain (RBD), and two S1 subdomains, SD1 and SD2. The RBD domain is observed in up and down conformations, accounting for >90% of the neutralizing activity in sera from COVID-19 convalescent and vaccinated individuals (6–9). Durable RBD-specific memory B cell and nAb responses are known to provide protection against COVID-19 (7, 10). RBD monomer, tandem RBD dimer, and RBD trimer induce potent Ab responses (11–13). Self-assembling multivalent RBD nanoparticles, facilitated by designed or scaffold proteins, further demonstrated extraordinarily high potentiation of immune responses (14–16).

Recent outbreaks of variants indicate a high degree of waning immunity, contributing to increased infectiousness and immune evasion (17–19). The new variants may be less vulnerable to the RBD-directed antibodies (20–22), and administration of a third dose of vaccines resulted in substantially lowered rates of confirmed cases and severe illness (16). With the repeated booster vaccination, however, it was suggested that immunological imprinting directed toward strain-specific antigens may lead to overspecialization of immunodominant B cells with limited breadth (23). In contrast, codisplay of heterologous RBDs on nanoparticles showed an avidity advantage to cross-reactive B cells, eliciting broader Ab responses than a mixture or cocktail of nanoparticles (23–25). These innovative platforms prepared by designed scaffold, sortase A, or Spy-tag-mediated fusion chemistry induce high immunogenicity and enhanced B cells with sufficient breadth. However, the platforms have significant drawbacks associated with employing a mixture of antigen-fused tags or scaffolds to assemble mosaic nanoparticles. Codisplay of heterologous RBDs will be more challenging in mass production, due to the difficulty to achieve a uniform distribution of antigens on nanoparticles.

In this study, we embraced an approach that a self-assembling scaffold, proliferating cell nuclear antigen (PCNA), can form nanoparticles uniformly incorporating heterotypic antigens. PCNA is a ring-shaped protein that encircles DNA as a processivity factor (26–28). Most organisms encode a homotrimeric PCNA from bacteria to higher

Significance

Despite the arsenal of COVID-19 vaccines, hospitalization and mortality associated with severe acute respiratory syndrome coronavirus-2 (SARS-CoV-2) remain high. There is an urgent need to develop next-generation vaccines that provide broad protection against diseases caused by newly emerging variants. In this study, six receptor-binding domains (RBDs) derived from α- and β-CoV were linked to proliferating cell nuclear antigen heterotrimeric scaffolds, to create a mosaic multivalent nanoparticle, 6RBD-np. Immunization in human angiotensin-converting enzyme 2–transgenic mice with 6RBD-np elicited consistently high antibody responses against RBD antigens derived from the α- and β-CoV and full protection against the SARS-CoV-2 challenges. This study provides proof of concept that the mosaic 6RBD-np induces 100% protection against SARS-CoV-2 challenges with the potential to induce intergenus cross-reactivity.

The authors declare no competing interest.

This article is a PNAS Direct Submission.

[1]D.B.L., H.K., and J.H.J. contributed equally to this work.

[2]To whom correspondence may be addressed. Email: mschung@duksung.ac.kr, microuni@chungbuk.ac.kr, or khkim@korea.ac.kr.

This article contains supporting information online at https://www.pnas.org/lookup/suppl/doi:10.1073/pnas.2208425120/-/DCSupplemental.

Published January 20, 2023.

eukaryotes, including humans, whereas a hyperthermophilic archaea, *Saccharolobus solfataricus*, possesses a heterotrimeric PCNA. Six RBDs derived from α- and β-CoV were attached to PCNA subunits, to form a mosaic multivalent nanoparticle, 6RBD-np. It elicited significantly high Ab titers against the RBD antigens derived from α- and β-CoV and increased interferon (IFN-γ) production, suggesting the potential to induce intergenus cross-reactivity.

Results

Design and Assembly of Mosaic Nanoparticle 6RBD-np. To overcome the common disadvantages of mosaic nanoparticle platforms relying on the stochastic assembly (22–25), a heterotrimeric PCNA from *S. solfataricus* was chosen as a scaffold with three subunits (PCNA1, PCNA2, and PCNA3). The PCNA subunits of ~250 amino acids have similar structures, despite their low sequence similarity (8 to 22%) and are assembled in a sequential manner: PCNA1 and PCNA2 dimerize and recruit PCNA3 to form a heterotrimer, with dissociation constants in micromolar to nanomolar ranges (26–29).

RBD-targeting nAbs provide the highest neutralizing potencies when targeting conserved epitopes of RBD in the down conformation. The presence of SD1 stabilizes the RBD-down conformation, which can also be critical for stability of spike proteins (30–32). Six RBD-SD1s were thus selected, derived from α- and β-CoV that are considered to have caused zoonotic infections (3, 4): residues from 319 to 592 for SARS-CoV-2 wild-type (WT) and variant (VAR), 306 to 578 for SARS-CoV, 367 to 657 for MERS-CoV, 313 to 674 for hCoV HKU1, and 284 to 499 for hCoV 229E spike RBD-SD1s (Fig. 1*A*). The RBD-SD1 of SARS-CoV-2 VAR included the K417N, L452R, T478K, E484K, and N501Y mutations, covering RBD mutations in the variants, Alpha to Delta. The RBD-SD1 antigens derived from the six CoVs were incorporated into the N terminus and C terminus of PCNA1, PCNA2, and PCNA3 via an SGG linker, to construct the fusion protein components for assembly: (SARS-CoV-2 WT RBD-SD1)-PCNA1-(SARS-CoV RBD-SD1), (MERS-CoV RBD-SD1)-PCNA2-(SARS-CoV-2 VAR RBD-SD1), and (hCoV 229E RBD-SD1)-PCNA3-(hCoV HKU1 RBD-SD1), which were termed S-PCNA1, M-PCNA2, and H-PCNA3, respectively (Fig. 1*B*).

The fusion components, S-PCNA1, M-PCNA2, and H-PCNA3, were expressed in HEK 293F cells and purified using His-tag affinity, ion exchange, and size exclusion chromatography (SEC) (*SI Appendix*, Fig. S1*A*). They were mixed in a sequential order to generate mosaic multivalent nanoparticles, 6RBD-np (*SI Appendix*, Figs. S1*B* and S2*A*), showing the intersubunit dissociation constants of S-PCNA1 and M-PCNA2 followed by H-PCNA3 for assembly of 1×10^{-12} and $1 \times 10^{-(6\text{–}7)}$, respectively (*SI Appendix*, Table S1).

Uniform Assembly of 6RBD-np with Heterologous Antigens. Purified S-PCNA1, M-PCNA2, H-PCNA3, and 6RBD-np were subjected to SDS-PAGE and western blot with anti-His-tag monoclonal Ab (mAb), anti-SARS-CoV-2 spike polyclonal Ab (pAb), and anti-HKU1 spike mAb (Fig. 2*A*). All the antigens were detected by the anti-His-tag mAb. However, H-PCNA3, composed of two hCoV RBDs, was not detected by anti-SARS-CoV-2 spike pAb. 6RBD-np and H-PCNA3 were detected by the anti-HKU1 spike mAb, whereas S-PCNA1 and M-PCNA2 were not. It is notable that the number of protein bands on western blot detected by the anti-His-tag, anti-SARS-CoV-2, and anti-HKU1 Abs were 3, 2, and 1, respectively (Fig. 2*A* and *SI Appendix*, Fig. S2*B*).

The purified antigens were characterized by SEC-MALS: S-PCNA1, M-PCNA2, H-PCNA3, and 6RBD-np showed molecular weights of 154.0 kDa (±12.2%), 182.2 kDa (±1.8%), 175.8 kDa (±1.6%), and 355.7 kDa (±3.6%), respectively (Fig. 2*B* and *SI Appendix*, Fig. S3). The 6RBD-np was further examined by atomic force microscopy (AFM) and transmission electron microscopy (TEM). A ring-shaped scaffold structure with six protruding RBD-SD1 antigens was clearly observed, having an overall size of 40 nm (Fig. 2 *C* and *D*). biolayer interferometry was used to monitor the binding affinities of monomeric hACE2 ectodomain to 6RBD-np, showing a dissociation constant (K_D) of 2.5×10^{-7}, and to each component (Fig. 2*E* and *SI Appendix*, Table S2 and Fig. S4).

Stability of Mosaic 6RBD-np. The stability of the fusion components and 6RBD-np was monitored at −80 °C, 4 °C, 25 °C, and 37 °C over a 28-d storage period. They were resistant to degradation at −80 °C over 28 d (Fig. 3*A* and *SI Appendix*, Fig. S5). Incubation at 4 °C showed excellent stability, and partial degradation started on day 28 in S-PCNA1 only. In contrast, severe degradation was observed at 25 °C after 4 d of incubation and at 37 °C after 1 d of incubation. When the stability was examined using SEC after 30 d, the 6RBD-np and H-PCNA3 were found to be stable for more than 30 d at 4 °C (Fig. 3*B* and *SI Appendix*, Fig. S6). 6RBD-np is equally or more stable upon assembly than the components, representing a stable mosaic multivalent nanoparticle.

6RBD-np Induces Broad Immune Responses Against SARS-CoV-2 Variants. Immunogenicity of the antigens was evaluated in BALB/c mice who received intramuscular prime-boost immunizations with a 3-wk interval (5 μg antigen per mouse). Blood samples were collected at three time points: before immunization (preprime) and 2 wk after prime and boost immunizations (prime and boost) (Fig. 4*A*). The mice were divided into six groups of RBD-SD1 of SARS-CoV-2, spike ectodomain with two proline substitutions (S-2P) of SARS-CoV-2, S-PCNA1, and 6RBD-np (n = 10), and the naive and PCNA controls (n = 5). When postboost sera were analyzed with the SARS-CoV-2 RBD-SD1, the S-PCNA1 and 6RBD-np groups showed the highest Ab titers, followed by the RBD-SD1 and S-2P groups (Fig. 4 *A*, *Middle*). The results suggest that both the 6RBD-np and S-PCNA1 groups showed significant and robust Ab responses, compared with the others. When the Ab responses in the postboost sera were compared with respect to dosage (15 μg vs. 5 μg) and adjuvants (Sigma adjuvant system (SAS), AddaVax, and CpG-ODN), the 15 μg (3×) 6RBD-np group achieved the highest Ab response (Fig. 4 *A*, *Lower*). No significant difference was observed among the adjuvant groups.

We then assessed antigen-specific Ab titers in sera, using purified RBD-SD1s of SARS-CoV-2 (WT and VAR), SARS-CoV, and hCoVs HKU1 and RBDs of MERS-CoV and hCoV 229E (see *Methods*). The groups of S-PCNA1 and 6RBD-np showed distinctly high Ab titers against the SARS-CoV-2 (WT and VAR) and SARS-CoV antigens (Fig. 4*B*). The 6RBD-np group also displayed high Ab titers against the MERS-CoV, hCoV HKU1, and 229E antigens. We also assessed anti-SD1 IgG titers in sera, using recombinant SD1s, which were mostly lower than those against RBD-SD1s (*SI Appendix*, Fig. S7). Further, neutralizing activities of the mice sera against pseudoviruses encoding the spike of SARS-CoV and spike mutants of SARS-CoV-2 were determined. The 6RBD-np group neutralized the entry of pseudoviruses, expressing spike protein of SARS-CoV-2 D614G (Wuhan), Delta, bat CoV RaTG13, or SARS-CoV, or that with N532A or E554A/N556A (SD1) mutations, with high efficacy (Fig. 4*C* and *SI Appendix*, Fig. S8). Our data suggest that the Abs in the 6RBD-np group

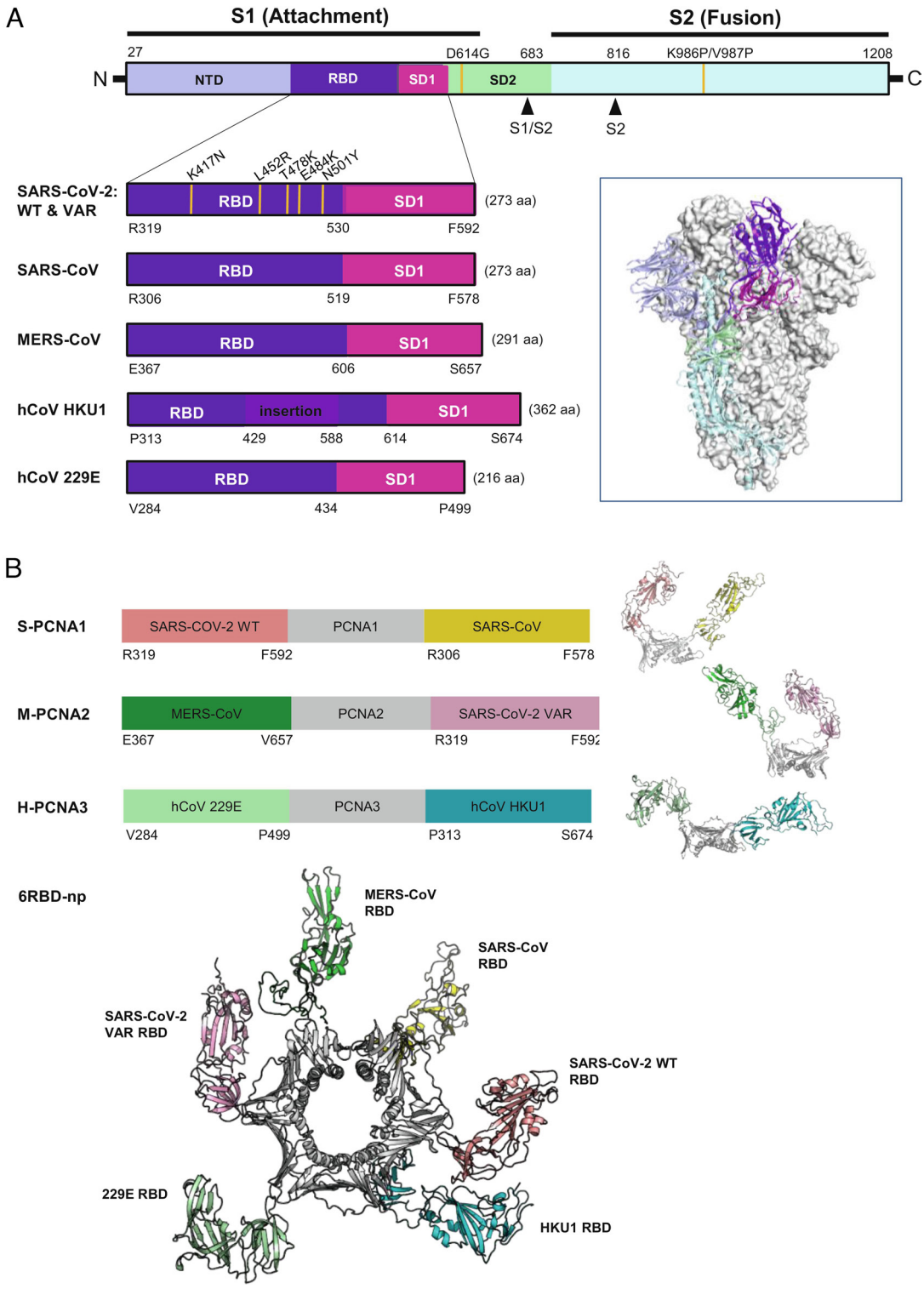

Fig. 1. Design and characterization of 6RBD-np antigen. (*A*) Schematic of SARS-CoV-2 spike primary structure colored by domains. It is composed of the S1 region containing NTD, RBD, and SD1 and SD2, and the S2 region. The mutation sites for SARS-CoV-2 VAR are indicated by yellow vertical lines. The RBD and SD1 regions are derived from 319 to 592 for SARS-CoV-2 WT and variant, 306 to 578 for SARS-CoV, 367 to 657 for MERS-CoV, 313 to 674 for hCoV-HKU1, and 284 to 499 for hCoV-229E spike proteins. A prefusion trimeric structure of SARS-CoV-2 spike protein is shown on the right. A single protomer is shown in ribbon representation and colored as in the primary structure diagram. The two remaining protomers are shown as the molecular surface in gray. (*B*) Design of S-PCNA1, M-PCNA2, and H-PCNA3 showing schematic diagrams of CoV spike RBD-SD1-PCNA fusion proteins (*Upper*): S-PCNA1, (SARS-CoV-2 WT RBD-SD1)-PCNA1-(SARS-CoV RBD-SD1); M-PCNA2, (MERS-CoV RBD-SD1)-PCNA2-(SARS-CoV-2 VAR RBD-SD1); H-PCNA3, (hCoV 229E RBD-SD1)-PCNA3-(hCoV HKU1 RBD-SD1). Composite molecular models of S-PCNA1, M-PCNA2, and H-PCNA3 are shown on the right. A molecular model of 6RBD-np displaying PCNA ring (gray) and six RBD-SD1 proteins colored as in the schematic diagram (*Lower*). The RBD-SD1s are fused to the PCNA subunits, such that the SD1s are close to the PCNA ring, whereas the RBDs are exposed on the external surface of the nanoparticle. The models were generated from structures of PDB IDs: 6VXX, 5W9P, 5X5B, 6U7H, 5I08, and 2HIK for SARS-CoV-2, MERS-CoV, SARS-CoV, hCoV 229E, and hCoV HKU1 spike proteins, and PCNA, respectively.

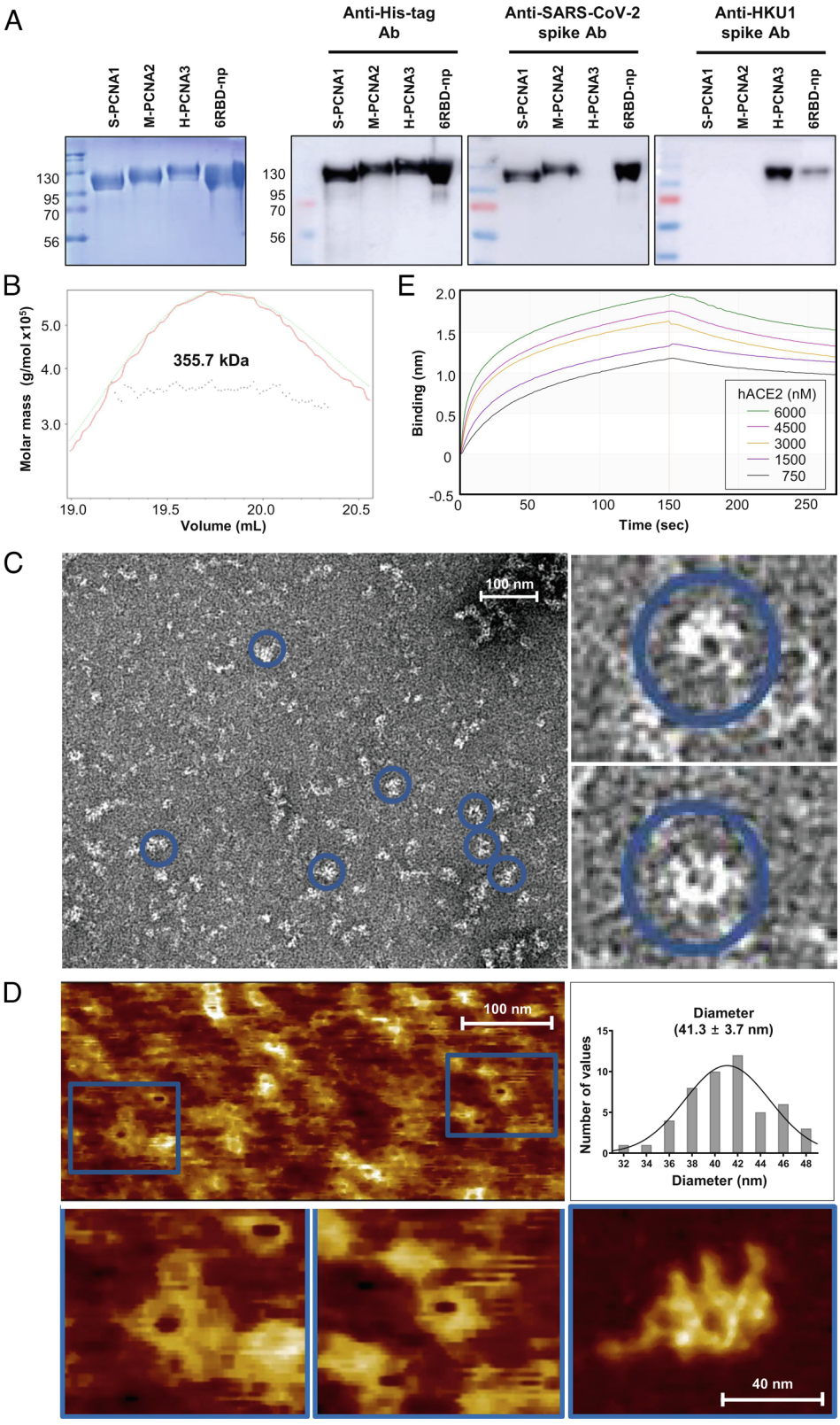

Fig. 2. Antigenic and biophysical characterization of 6RBD-np. (*A*) SDS-PAGE and western blot assay results of the purified components, S-PCNA1, M-PCNA2, H-PCNA3, and 6RBD-np using anti-His-tag mAb, anti-SARS-CoV-2 spike pAb, and anti-hCoV HKU1 spike mAb. (*B*) Purified 6RBD-np was characterized using SEC-MALS to show its molecular weight of 355.7 kDa (±3.6%). (*C*) Negative staining electron (TEM) micrographs and (*D*) AFM images of the 6RBD-np with scale bars of 100 nm. The circles on the right (*C*) and rectangles below (*D*) are magnified TEM and AFM images of 6RBD-np, respectively. The histogram of the diameter of 6RBD-np, on the right, was prepared with 50-line profile data, based on AFM images, and a high-resolution image is shown at a scale of 40 nm (right below). (*E*) Determination of binding affinities between hACE2 and 6RBD-np by biolayer interferometry. Analysis of monomeric hACE2 binding to immobilized 6RBD-np was performed using Ni-NTA biosensors.

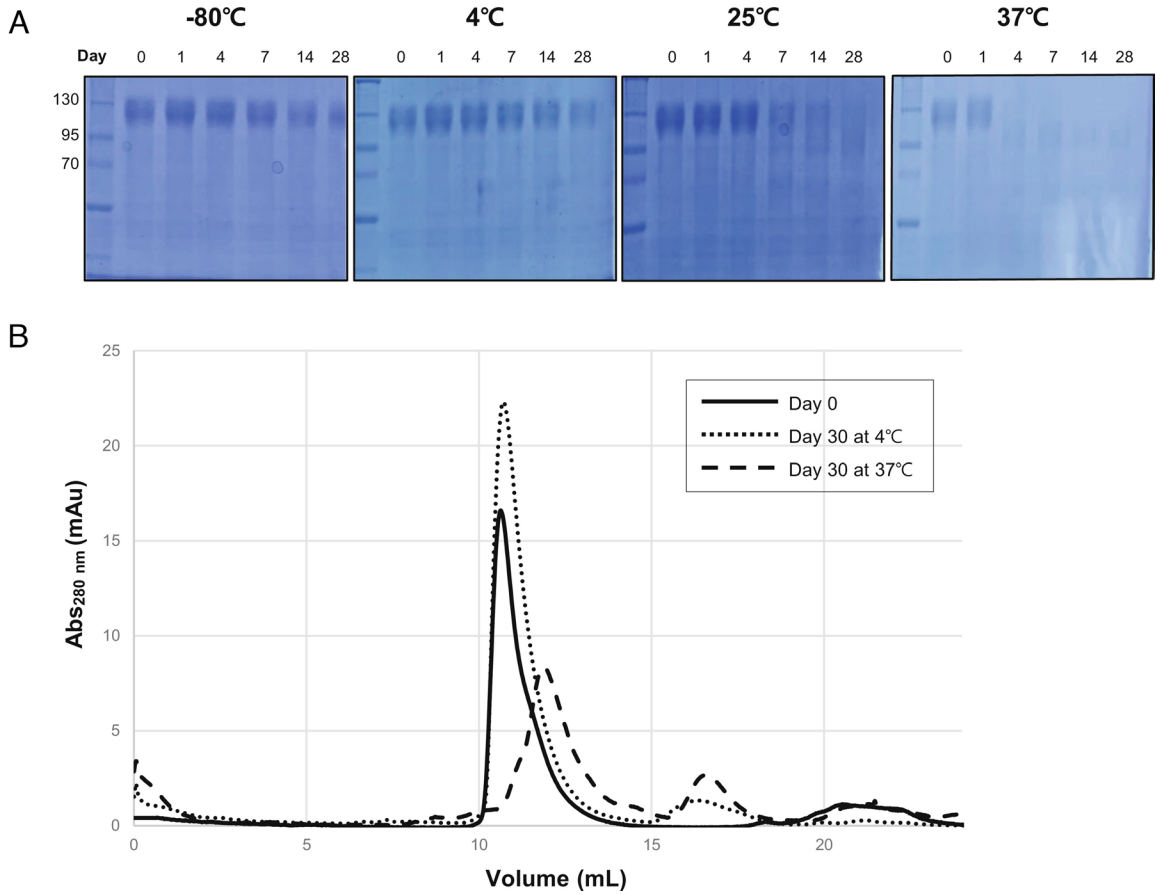

Fig. 3. Time-course stability of 6RBD-np. (*A*) SDS-PAGE and (*B*) SEC results monitored at −80 °C, 4 °C, 25 °C, and 37 °C over a 28-d storage period. (*A*) The left lane indicates molecular weight markers and following lanes monitored on days 0, 1, 4, 7, 14, and 28. (*B*) Elution profiles of 6RBD-np, obtained on day 0 (continuous line) and 30 at 4 °C (dotted) and 37 °C (dashed), after SEC on Superdex 200 increase 10/300 GL.

neutralized cell entry of pseudoviruses efficiently, irrespective of RBD and SD1 mutations and irrespective of SARS-CoV, bat CoV RaTG13, and SARS-CoV-2 spikes used in this study.

We also assessed nAb titers in sera, using the WT, Delta, and Omicron (BA.1) viruses. The 6RBD-np group demonstrates high neutralizing potency against the authentic viruses, from the WT to the variants (Fig. 4*D*). The neutralizing potency of 6RBD-np was higher than or comparable to that of the convalescent sera from a COVID-19 positive. Thus, the immunogenicity of the 6RBD-np in mice sera was significantly high both in the pseudovirus-based and authentic virus-based neutralization assays, as shown in Fig. 4 *C* and *D*, respectively.

6RBD-np Completely Protects Mice Against SARS-CoV-2 WT and Delta Challenges. To evaluate the immunogenicity and protective efficacy of the antigens against the SARS-CoV-2 WT and Delta challenges, hACE2 knock-in mice were given intramuscular prime-boost immunizations with a 3-wk interval (5 μg antigen per mouse) (Fig. 5*A*): six groups of RBD-SD1 of SARS-CoV-2, S-2P of SARS-CoV-2, S-PCNA1, 6RBD-np (n = 10 each for the WT and Delta challenges), naive (n = 6), and virus control (n = 8 each for the WT and Delta) groups. At 3 wk postboost, all groups except for the naive group were challenged with intranasal inoculation of 10 MLD_{50} of SARS-CoV-2 WT or Delta variant. The S-2P, S-PCNA1, and 6RBD-np groups exhibited survival rates of 100% against the WT challenge, whereas the RBD-SD1 and 6RBD-np groups survived at the same rates against the Delta challenge (Fig. 5 *A*, *Middle* and *Lower*). No significant changes in body weights were observed in the 6RBD-np group, the only group showing survival rates of 100%, irrespective of WT or Delta challenge. The S-2P and S-PCNA1 groups exhibited average survival rates of 86% and 71% against Delta, respectively, while the RBD-SD1 group showed a survival rate of 57% against the WT challenge, exhibiting significant body weight loss.

When the viral titers were measured in the lung and brain tissues collected at 5 d postinfection (dpi), the lowest titers were observed in the 6RBD-np and naive groups against the WT and Delta challenges (Fig. 5*B*). The viral titers were partially inhibited in the RBD-SD1, S-2P, and S-PCNA1 groups. The mice in the immunized groups exhibited less severe histopathological lesions of interstitial pneumonia and lower N proteins, detected by immunohistochemistry (IHC), than those in the virus control group (*SI Appendix*, Fig. S9). The RBD-SD1 group, showing a 100% survival rate against the Delta challenge, revealed much higher histopathological damage and N proteins in the lung, compared to the 6RBD-np group. We assessed nAb titers in postboost sera, using the WT and Delta viruses. The S-PCNA1 and 6RBD-np groups revealed high neutralizing potency and breadth against the challenges (Fig. 5*C*).

6RBD-np Elicits Strong and Broad Ab and IFN-γ Responses. The antigen-specific Ab titers in sera, collected at three time points of postprime, postboost, and postchallenge with WT or Delta, were examined using different antigens. The S-PCNA1 and 6RBD-np immunogens induced high Ab titers against the SARS-CoV-2 and SARS-CoV antigens (Fig. 5*D*). The 6RBD-np group also showed

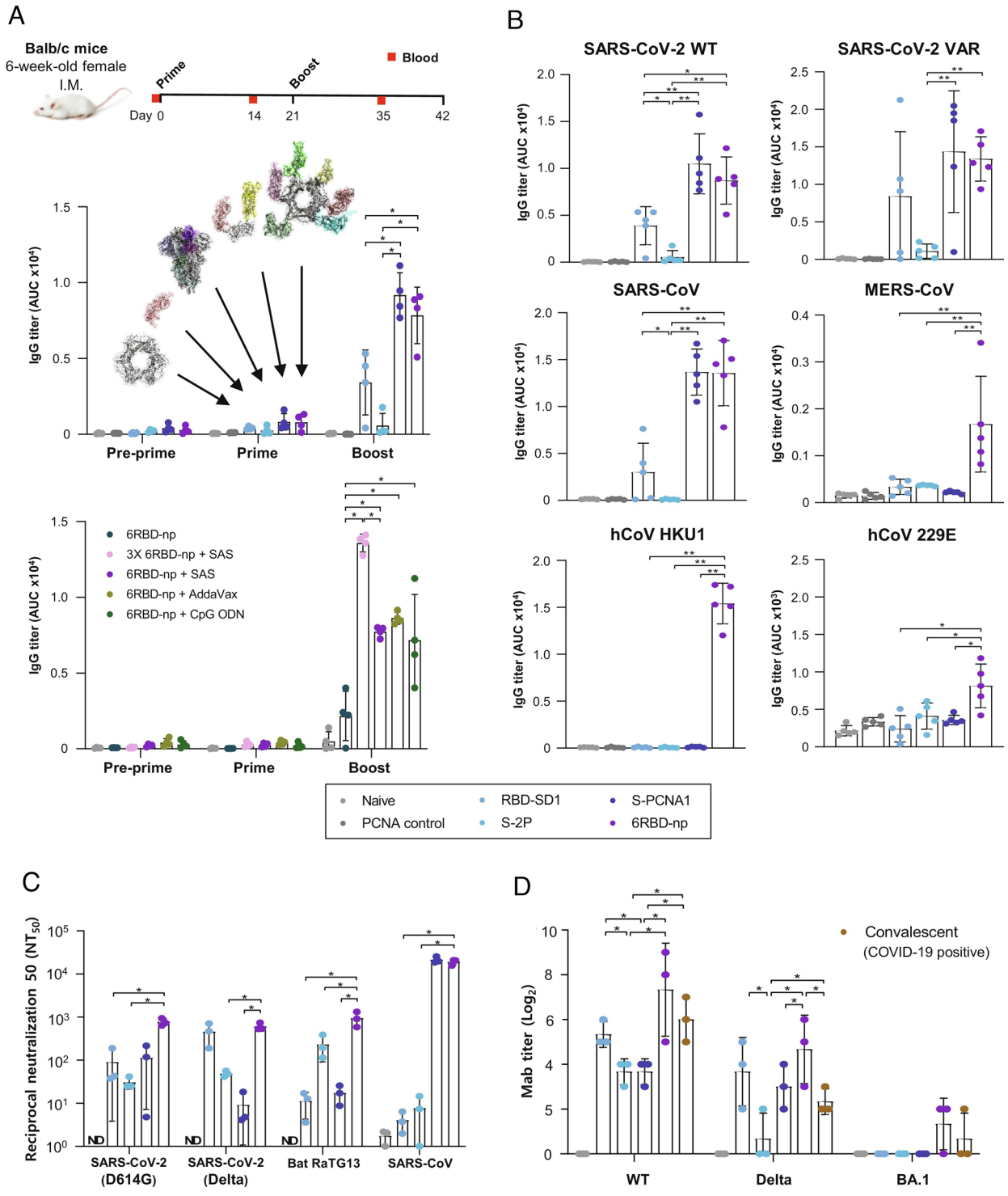

Fig. 4. Immunogenicity of antigens in BALB/c mice. (*A*) Design of prime-boost immunization studies with BALB/c mice (*Upper*). The mice were immunized intramuscularly with 5 μg of antigen in six groups: four antigen groups (n = 10) and the naive and PCNA controls (n = 5). Blood was collected before immunization (preprime) and 2 wk after prime and boost immunizations (prime and boost). Anti-RBD Ab titers were monitored against the purified RBD-SD1 of the SARS-CoV-2, for different antigen groups of the naive and PCNA controls, RBD-SD1 of SARS-CoV-2, S-2P of SARS-CoV-2, S-PCNA1, and 6RBD-np, represented as molecular structures of the respective antigens with arrows (*Middle*). Additional experiments were performed for different doses and adjuvants (*Lower*), in groups of 5 μg and 15 μg (3×) of 6RBD-np, 5 μg of 6RBD-np in the presence of SAS, AddaVax, and CpG-ODN. (*B*) postboost anti-RBD Ab titers against the antigens of the SARS-CoV-2 (WT and VAR), SARS-CoV, MERS-CoV, and hCoVs HKU1 and 229E. ELISA plates were coated with RBD-SD1s (SARS-CoV-2 WT or VAR, SARS-CoV, MERS-CoV, or hCoV HKU1) or RBD (hCoV 229E), serially diluted mouse sera, including naive mouse serum, and incubated for 1 h at room temperature. The absorbance of each well was measured at 450 nm, and ELISA data from serum IgG responses are shown as AUC (*A* and *B*). (*C*) Pseudovirus-based neutralization activities. Pseudoviruses expressing spike protein of SARS-CoV-2 D614G (Wuhan), Delta, bat CoV RaTG13, or SARS-CoV were inoculated with sera from the naive control, RBD-SD1 and S-2P of SARS-CoV-2, S-PCNA1, and 6RBD-np groups, which were serially diluted prior to transduction on HEK293T-hACE2 cells. Neutralization was performed in triplicates and data plotted and fit in Prism 9 (GraphPad) using nonlinear regression sigmoidal, to determine IC_{50} values from curve fits. ND: nondetectable. (*D*) Authentic virus-based neutralization activities. NAb titers in sera were measured using the WT, Delta, and Omicron (BA.1) viruses. SARS-CoV-2 viruses (WT, Delta, or Omicron BA.1 variant) at 10^2 $TCID_{50}$/50 μL were mixed with diluted serum at a 1:1 ratio prior to 1-h incubation at 37 °C. Convalescent sera from a COVID-19-positive individual were also used as a positive control. Mean neutralization Ab titers were calculated and compared. In (*A*–*D*), data were compared using the Mann–Whitney *U* test (*$P < 0.05$; **$P < 0.01$). The mean values are indicated by a bar or a short horizontal line, where each value from individual mice sera is presented as a symbol, and the SD is indicated by a vertical line. Statistically significant differences are indicated only among different immunogen groups.

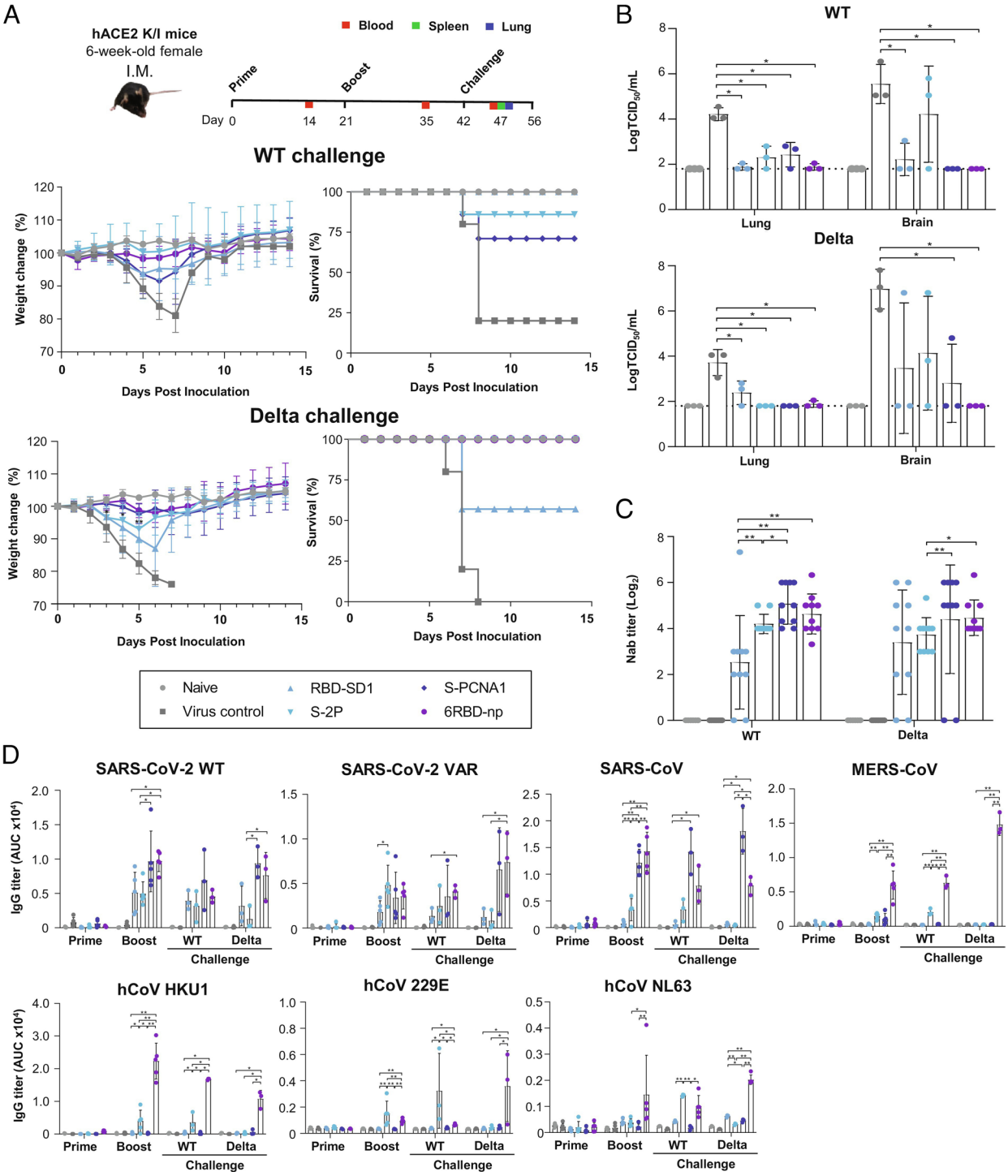

Fig. 5. Protective efficacy and immunogenicity of antigens against SARS-CoV-2 WT and Delta challenges in hACE2 transgenic mice. (*A*) Design of prime-boost immunization and challenge studies with hACE2 transgenic mice (*Upper*). The challenge experiment was performed at the BSL3 animal facility of Chungbuk National University, where two independent animal challenge experiments were performed using 10 mice each for the SARS-CoV-2 WT and Delta variant challenges. Mice were given 5 μg of antigen intramuscularly. Weight loss and survival of hACE2 transgenic mice, following the SARS-CoV-2 WT or Delta challenge, were monitored up to 14 d postinfection (dpi), in six groups of the SARS-CoV-2 RBD-SD1, S-2P, S-PCNA1, 6RBD-np, naive, and virus-infected control (*Middle* and *Lower*): groups of RBD-SD1, S-2P, S-PCNA1, and 6RBD-np (n = 10 each for the WT and Delta) and of naive (n = 6) and virus control (n = 8 each for the WT and Delta). Mice in the virus control group inoculated intranasally with the WT or Delta challenge started to lose weight at 2 or 3 dpi, respectively, showing rapid body weight loss and decline in survival rates. Data for weight changes between the S-2P and 6RBD-np groups in the WT challenge were compared on days 3 to 5, using the Mann–Whitney *U* test (**P* < 0.05; ***P* < 0.01), which showed significant differences of weight changes between the two groups. (*B*) Viral titers in mice lungs and brain, collected from 3 mice per group, obtained 5 dpi, following the SARS-CoV-2 WT or Delta challenge with 10 MLD_{50}, expressed in log $TCID_{50}$/mL. Frozen tissues were homogenized, and the supernatant was used to infect cells (1.5×10^4/well) in 96-well plates. Virus-induced CPE were measured. (*C*) NAb titers in mice sera collected at 2 wk postboost against the WT and Delta viruses. SARS-CoV-2 viruses (WT or Delta variant) at 10^2 $TCID_{50}$/50 μL were mixed with diluted serum at a 1:1 ratio prior to 1-h incubation at 37 °C. Mean nAb titers were calculated and compared. (*D*) Anti-RBD Ab titers in mice sera 2 wk after prime and boost and 5 d after challenges with the WT and Delta viruses, using ELISA assays. The antigens, RBD-SD1s (SARS-CoV-2 WT or VAR, SARS-CoV, MERS-CoV, hCoV HKU1, or hCoV NL63) or RBD (hCoV 229E), were incubated with serially diluted mouse sera, including naive mouse serum, for 1 h at room temperature. The absorbance of each well was measured at 450 nm, and ELISA data from serum IgG responses are shown as AUC. In (*B–D*), the data were compared using the Mann–Whitney *U* test (**P* < 0.05; ***P* < 0.01). The mean values are indicated by a bar, where each value from individual mice sera is presented as a symbol, and the SD is indicated by a vertical line. Statistically significant differences are indicated only among different immunogen groups.

significantly high Ab titers against the MERS-CoV and hCoV HKU1 antigens, and the S-2P and 6RBD-np groups achieved significantly high Ab titers against hCoV 229E (an α-CoV). We then assessed the breadth of Ab responses by the codisplay of heterologous antigens, using the RBD of hCoV NL63 (an α-CoV), which is not included in the antigens. High Ab titers against the NL63 RBD were induced by the S-2P and 6RBD-np groups, showing similar responses to those against the 229E RBD (Fig. 5*D*).

We also measured T cell responses using interferon (IFN)-γ ELISpot assays in mice splenocytes, following stimulation with a pool of 53 overlapping 15-mer peptides spanning the SARS-CoV-2 WT RBD. Compared to the RBD-SD1, S-2P, and S-PCNA1 groups, the 6RBD-np group was found to induce higher IFN-γ-producing T cell responses (*SI Appendix*, Fig. S10). Together, our results demonstrate that 6RBD-np induced significantly high Ab titers against the RBD antigens derived from α- and β-CoV and increased IFN-γ production, suggesting the potential to induce intergenus cross-reactivity.

Discussion

Multiple variants of SARS-CoV-2, including Delta (B.1.617.2) and Omicron (B.1.1.529), have been identified globally during the pandemic (20–21, 22). The Omicron variant, harboring 37 amino acid changes to the spike protein, has substantially increased the ability to evade immunity from vaccination or prior infection (33–35). The emergence of immune-evading variants is a global concern (36), although an arsenal of COVID-19 vaccines provides partial protection against the multiple variants (37–40). Notably, the current vaccines are primarily directed toward the viral spike protein, specifically focused on receptor interaction. As a vaccine-induced immune response, nAbs targeting the RBD of SARS-CoV-2 are still considered a crucial correlate of protection against COVID-19 (9, 41). The RBD accounts for more than 90% of the neutralizing activity in sera from convalescent and vaccinated individuals (6–9). RBD monomer, dimer, and trimers have indeed been shown to elicit potent Ab responses (6, 7, 10). Self-assembling multivalent RBD or spike nanoparticles, using SpyTag/SpyCatcher or sortase-mediated ligation and computationally designed scaffolds, ferritin, or lumazine synthase fusion platforms, have shown high potentiation of immune responses against COVID-19 (14, 15, 16–44). However, administration of homotypic multivalent antigens or possibly multiple booster doses with strain-specific antigens can lead to overspecialization of the B cells with limited breadth of antigen recognition (23). In contrast, mosaic nanoparticles achieved by mixing heterologous β-CoV RBDs provide an avidity advantage to elicit superior cross-reactive B cells than an admixture of nanoparticles (24, 25).

A current formulation of mosaic nanoparticles with a uniform distribution of heterotypic antigens, however, cannot be reliably prepared by direct mixing, and quality assurance in mass production will be more challenging in human trials. In this study, six heterologous RBD-SD1s are fused to the termini of PCNA1, PCNA2, and PCNA3, which are self-assembled in a defined order to form 6RBD-np, with dissociation constants in micromolars to nanomolars. The nanoparticle was characterized to show a ring-shaped disk with six protruding RBD-SD1s with an overall size of 40 nm, like jewels in a crown. Antigenic characterization revealed that six heterologous antigens are uniformly distributed on 6RBD-np, strongly suggesting that the PCNA subunits possess an important advantage over the current stochastic assembly platforms in the formulation of mosaic multivalent antigens.

In BALB/c mice, the 6RBD-np group demonstrated high Ab titers for each antigen in postboost sera in a dose–response manner. In hACE2 transgenic mice, as shown in Fig. 5, the prime-boost immunization of the 6RBD-np induced protective immunity against the SARS-CoV-2 WT and Delta challenges, which was the only group with 100% survival rates among the antigen groups. The 6RBD-np elicited significantly high nAb titers in pseudovirus-based and authentic virus-based neutralization assays, demonstrating broad and potent serum neutralization capacity. Notably, the S-PCNA1 and 6RBD-np groups exhibited higher Ab titers in the challenged sera against the RBDs derived from SARS-CoV and SARS-CoV-2, compared to other groups, possibly due to the presence of the SARS-CoV and SARS-CoV-2 RBDs in the antigens. While the 6RBD-np group showed high Ab titers against the RBDs of MERS and hCoVs HKU1, the S-2P and 6RBD-np groups showed high titers against those of 229E and NL63. The elevated Ab levels in the S-2P group against 229E and NL63 RBDs, albeit in the WT challenge only, are likely to reflect the importance of antigen size (S-2P and 6RBD-np are the largest among the antigens in this study), when the antigen carries little antigenicity common to the α-CoV RBD. S-2P may also be a good humoral immunogen against hCoVs to provide underlying conserved epitopes in hCoV RBDs (e.g., at monomer–monomer interfaces). Nevertheless, the mosaic 6RBD-np, having five β-CoV RBDs and an α-CoV RBD, is shown to induce potent Ab responses in sera against the RBDs from α- and β-CoV in this study, including, surprisingly, the hCoV NL63 RBD.

The RBDs show distinctly different sizes and structures (*SI Appendix*, Fig. S11). The β-CoVs, SARS-CoV-2, SARS-CoV, MERS-CoV, and hCoV HKU1, share a five-stranded antiparallel β-sheet and extended loops of receptor-binding motifs, whereas the α-CoVs, hCoVs 229E, and NL63 share a β-sandwich of three-stranded β-sheets. Nevertheless, the six RBD structures, when superimposed, share a central β-sheet with different arrangements of extended loops. As an immunodominant target of nAbs, codisplay of heterologous RBDs can confer an advantage to cross-reactive B cells, eliciting broad Ab responses (23). The 6RBD-np showed high potency against bat CoV RaTG13 and Omicron (BA.1) variant in the pseudovirus as well as the authentic virus-based neutralization assays, covering antiviral spectrum from the SARS-CoV-2 WT and variants to bat CoV. In this context, the mosaic nanoparticle, 6RBD-np, might play a key role in achieving broad intergenus CoV immunity based on conformationally conserved epitopes, which requires additional study.

Efficient cellular uptake, entry, and retention at lymph nodes of antigens are crucial for improved immunogenicity and protection, which is influenced by the size of antigen nanoparticle platforms (44, 45). Self-assembled protein nanoparticles are defined as a material that has dimensions between 1 and 100 nm, exhibiting physical, chemical, or biological effects (46). The repetitive array of antigens on nanoparticles facilitates activation of multiple B cell receptors, additionally highlighting the importance of antigen density in memory immune responses (45, 47). Although discrepancies may arise, the ideal nanoparticle platform for immune responses would be 20 to 50 nm in diameter, with antigens spaced 30 nm apart (44). The 6RBD-np is indeed shown to have a size of ~40 nm with interantigen spacing of 20 to 30 nm. This design model of 6RBD-np can provide readily modifiable scaffolds to which a wide variety of viral antigen cargoes can be presented uniformly, up to six heterologous antigens. The modular platform of the self-assembled mosaic nanoparticle can be adopted to develop pan-CoV vaccines to combat future spillovers.

Materials and Methods

Design, Expression, and Purification of 6RBD-np. For the six RBD-SD1 proteins, the residues of SARS-CoV-2 WT and VAR, SARS-CoV, MERS-CoV, hCoV 229E, and hCoV HKU1 RBD-SD1 proteins as well as PCNA1, PCNA2, PCNA3_S170V were amplified as described in *SI Appendix*, Table S3. Fusion proteins, S-PCNA1, M-PCNA2, and H-PCNA3, were constructed with an SGG linker. The RBD-SD1 of SARS-CoV-2 VAR included K417N, L452R, T478K, E484K, and N501Y mutations. The fusion proteins were expressed in Expi293F cells and purified by Ni-NTA affinity chromatography, ion-exchange chromatography, and SEC. The purified S-PCNA1, M-PCNA2, and H-PCNA3 was sequentially mixed, and the assembled 6RBD-np was purified by SEC. Each RBD-SD1 and SD1 antigen was also constructed, expressed, purified, and used for enzyme-linked immunosorbent assay (ELISA).

Characterization of Antigens. Light scattering and refractive index were measured using the WYATT-787-TS miniDAWN system; negative-stained electron microscopic images were obtained under a Tecnai 20 transmission electron microscope operating at 120 kV, and the AFM data were acquired using Multimode-VIII at 0.3 Hz in a line. The binding of antigens to receptors was measured by biolayer interferometry. Fusion proteins and 6RBD-np were treated with Endo H for deglycosylation, and overall structures of RBDs were superimposed using the Coot (48).

Mouse Immunization and Pseudovirus-Based Neutralization Assay. BALB/c mice for groups (n = 10) of RBD-SD1, S-2P trimer, S-PCNA1, and 6RBD-np were immunized in a prime-boost protocol with a 3-wk interval, and the naive and PCNA controls were n = 5. Antigens (5 μg) were injected intramuscularly. Blood was collected preprime and 2 wk after prime and boost via facial vein puncture. Serum was heat-inactivated, centrifuged, and stored at −80 °C. IgG responses were evaluated by ELISA as area under the curve (AUC).

Replication-deficient murine retrovirus-based pseudoviruses were generated as previously described (49). HEK293T cells were transfected with plasmids encoding MLV gag/pol, spike protein of SARS-CoV-2 D614G, SARS-CoV-2 Delta, bat CoV RaTG13, or SARS-CoV, and firefly luciferase reporter. Quantitative RT-PCR was used to monitor pseudovirus titers.

Virus Challenge and Neutralization and ELISpot Assays. B6.Cg-Tg(K18-ACE2)2Prlmn/J mice were given with 5 μg of SARS-CoV-2 antigen (RBD-SD1, S-2P, S-PCNA1, or 6RBD-np) in intramuscular prime-boost immunization with a 3-wk interval. The mice were inoculated with 10 MLD_{50} of SARS-CoV-2 WT or Delta virus intranasally. Weight loss and survival rate were monitored, and lung and brain tissues were harvested at 5 dpi. Sera were collected via the retro-orbital plexus at 2 wk after prime and boost and 5 d postinfection. The supernatant of collected tissues was used to infect Vero E6 cells (1.5×10^4/well) in 96-well plates and processed for histopathological examination using hematoxylin-and-eosin and IHC staining.

Sera were mixed with SARS-CoV-2 virus (WT, Delta, or Omicron BA.1) at 10^2 $TCID_{50}$/50 μL and applied to Vero E6 cells in a 96-well plate (1.5×10^4 cells/well). NAb titers were defined as the reciprocal of the highest serum dilution that inhibited virus-induced cytopathic effects (CPE). Convalescent sera collected from COVID-19-positive individual donors (51zkxu, 0xl7bb, and 65fyp1) were used as a positive control. The SARS-CoV-2-induced CPE was measured, and the mean and SD (on a log2 scale) of neutralization titers were determined. To measure antigen-specific IFN-γ secretion, a mouse IFN-γ ELISpot assay was performed using splenocytes (2×10^5 cells/well) stimulated with 0.2 μg of PepMix™ SARS-CoV-2 RBD.

Data, Materials, and Software Availability. All study data are included in the article and/or *SI Appendix*. The data will be available upon publication.

ACKNOWLEDGMENTS. This work was supported by the National Research Foundation of Korea grants (NRF-2021R1A4A1028969 & NRF-2020R1A2B5B03096290, K.H.K.) and the Korea Health Technology R&D Project grants (HV20C0054, K.H.K.) through the Korea Health Industry Development Institute (KHIDI), funded by the Korea government (MSIT and MHW) and the KBRI basic research program (22-BR-01-03, J.Y.M.). The viruses, β-CoV/Korea/KCDC03/2020 (NCCP43326) and hCoV-19/South Korea/KDCA2950/2021 (NCCP43389), were provided by the National Culture Collection for Pathogens, Republic of Korea. We thank Dr. Giri Kotiguda for his initiation of a multivalent platform during an influenza vaccine development.

Author affiliations: [a]Department of Biotechnology & Bioinformatics, Korea University, Sejong 30019, South Korea; [b]Department of Food and Nutrition, Duksung Women's University, Seoul 01369, South Korea; [c]College of Medicine and Medical Research Institute, Chungbuk National University, Cheongju 28644, South Korea; [d]Interdisciplinary Graduate Program for Artificial Intelligence Smart Convergence Technology, Korea University, Sejong 30019, South Korea; [e]Department of Brain and Cognitive Sciences, Daegu Gyeongbuk Institute of Science and Technology, Daegu 42988, South Korea; [f]Laboratory for Biomedical Research, Ghent University Global Campus, Incheon 21985, South Korea; [g]Laboratory of Cellular and Molecular Immunology, Vrije Universiteit Brussel, Brussels 1050, Belgium; [h]Department of Biochemistry and Biotechnology, Ghent University, Ghent 9000, Belgium; [i]Department of Biomedical Molecular Biology, Ghent University, Ghent 9000, Belgium; and [j]Research Group for Neural Circuit, Korea Brain Research Institute, Daegu 41062, South Korea

Author contributions: M.S.C., Y.H.B., and K.H.K. designed research; D.B.L., H.K., J.H.J., U.S.J., Y.J., S.R., H.J., E.J.K., S.Y.H., J.Y.Ma., S.M., M.R., J.Y.Mu., H.S.J., G.L., M.-S.S., H.-R.L., M.S.C., Y.H.B., and K.H.K. performed research; D.B.L., H.K., J.H.J., U.S.J., Y.J., S.R., H.J., E.J.K., S.Y.H., J.Y.Ma., S.M., M.R., J.Y.Mu., H.S.J., G.L., M.-S.S., H.-R.L., M.S.C., Y.H.B., and K.H.K. analyzed data; and M.S.C., Y.H.B., and K.H.K. wrote the paper.

1. K. E. Jones *et al.*, Global trends in emerging infectious diseases. *Nature* **451**, 990–993 (2008).
2. L. H. Taylor *et al.*, Risk factors for human disease emergence. *Philos. Trans. R. Soc. Lond. B. Biol. Sci.* **356**, 983–989 (2001).
3. H. D. Marston *et al.*, Emerging viral diseases: Confronting threats with new technologies. *Sci. Transl. Med.* **6**, 253ps210 (2014).
4. J. Cui *et al.*, Origin and evolution of pathogenic coronaviruses. *Nat. Rev. Microbiol.* **17**, 181–192 (2019).
5. Q. Wang *et al.*, Structural and functional basis of SARS-CoV-2 entry by using human ACE2. *Cell* **181**, 894–904 (2020).
6. A. J. Greaney *et al.*, Antibodies elicited by mRNA-1273 vaccination bind more broadly to the receptor binding domain than do those from SARS-CoV-2 infection. *Sci. Transl. Med.* **13**, eabi9915 (2021).
7. P. K. Mishra *et al.*, Natural infection with SARS-CoV-2 generates durable Spike S1 Receptor-Binding-Domain-specific memory B cell and neutralizing antibody responses. *J. Immunol.* **206**, 19 (2021).
8. M. Jeyanathan *et al.*, Immunological considerations for COVID-19 vaccine strategies. *Nat. Rev. Immunol.* **20**, 615–632 (2020).
9. F. A. Krammer, correlate of protection for SARS-CoV-2 vaccines is urgently needed. *Nat. Med.* **27**, 1147–1148 (2021).
10. L. Piccoli *et al.*, Mapping neutralizing and immunodominant sites on the SARS-CoV-2 spike receptor-binding domain by structure-guided high-resolution serology. *Cell* **183**, 1024–1042. e1021 (2020).
11. J. Yang *et al.*, A vaccine targeting the RBD of the S protein of SARS-CoV-2 induces protective immunity. *Nature* **586**, 572–577 (2020).
12. L. Dai *et al.*, A universal design of betacoronavirus vaccines against COVID-19, MERS, and SARS. *Cell* **182**, 722–733 e711 (2020).
13. L. Yang *et al.*, A recombinant receptor-binding domain in trimeric form generates protective immunity against SARS-CoV-2 infection in nonhuman primates. *Innovation N Y)* **2**, 100140 (2021).
14. A. C. Walls *et al.*, Elicitation of potent neutralizing antibody responses by designed protein nanoparticle vaccines for SARS-CoV-2. *Cell* **183**, 1367–1382 (2020).
15. Y. F. Kang *et al.*, Rapid development of SARS-CoV-2 spike protein receptor-binding domain self-assembled nanoparticle vaccine candidates. *ACS Nano* **15**, 2738–2752 (2021).
16. K. O. Saunders *et al.*, Neutralizing antibody vaccine for pandemic and pre-emergent coronaviruses. *Nature* **594**, 553–559 (2021).
17. E. C. Wall, Neutralising antibody activity against SARS-CoV-2 VOCs B. 1.617. 2 and B. 1.351 by BNT162b2 vaccination. *Lancet* **397**, 2331–2333 (2021).
18. Y. Goldberg *et al.*, Waning immunity after the BNT162b2 vaccine in Israel. *N. Engl. J. Med.* **385**, e85 (2021).
19. B. Mizrahi *et al.*, Correlation of SARS-CoV-2-breakthrough infections to time-from-vaccine. *Nat. Commun.* **12**, 6379 (2021).
20. D. A. Collier *et al.*, Sensitivity of SARS-CoV-2 B.1.1.7 to mRNA vaccine-elicited antibodies. *Nature* **593**, 136–141 (2021).
21. M. McCallum *et al.*, SARS-CoV-2 immune evasion by the B.1.427/B.1.429 variant of concern. *Science* **373**, 648–654 (2021).
22. P. F. Wang *et al.*, Antibody resistance of SARS-CoV-2 variants B.1.351 and B.1.1.7. *Nature* **593**, 130–135 (2021).
23. M. Kanekiyo *et al.*, Mosaic nanoparticle display of diverse influenza virus hemagglutinins elicits broad B cell responses. *Nat. Immunol.* **20**, 362–372 (2019).
24. A. C. Walls *et al.*, Elicitation of broadly protective sarbecovirus immunity by receptor-binding domain nanoparticle vaccines. *Cell* **184**, 5432–5447 (2021).
25. A. A. Cohen *et al.*, Mosaic nanoparticles elicit cross-reactive immune responses to zoonotic coronaviruses in mice. *Science* **371**, 735–741 (2021).
26. I. Dionne, R. K. Nookala, S. P. Jackson, A. J. Doherty, S. D. Bell, A heterotrimeric PCNA in the hyperthermophilic archaeon Sulfolobus solfataricus. *Mol. Cell* **11**, 275–282 (2003).
27. G. J. Williams *et al.*, Structure of the heterotrimeric PCNA from Sulfolobus solfataricus. *Acta Crystallogr. Sect. F Struct. Biol. Cryst. Commun.* **62**, 944–948 (2006).
28. V. Hlinkova *et al.*, Structures of monomeric, dimeric and trimeric PCNA: PCNA-ring assembly and opening. *Acta Crystallogr. D Biol. Crystallogr.* **64**, 941–949 (2008).
29. C. K. Tan *et al.*, An auxiliary protein for DNA polymerase-delta from fetal calf thymus. *J. Biol. Chem.* **261**, 12310–12316 (1986).
30. L. Liu *et al.*, Potent neutralizing antibodies against multiple epitopes on SARS-CoV-2 spike. *Nature* **584**, 450–456 (2020).

31. P. J. M. Brouwer *et al.*, Potent neutralizing antibodies from COVID-19 patients define multiple targets of vulnerability. *Science* **369**, 643–650 (2020).
32. D. F. Robbiani *et al.*, Convergent antibody responses to SARS-CoV-2 in convalescent individuals. *Nature* **584**, 437–442 (2020).
33. J. R. Pulliam *et al.*, Increased risk of SARS-CoV-2 reinfection associated with emergence of the Omicron variant in South Africa. *Science* **376**, eabn4947 (2022), 10.1126/science.abn4947.
34. R. Pajon *et al.*, SARS-CoV-2 omicron variant neutralization after mRNA-1273 booster vaccination. *N. Engl. J. Med.* **386**, 1088–1091 (2022).
35. M. McCallum *et al.*, Structural basis of SARS-CoV-2 omicron immune evasion and receptor engagement. *Science* **375**, 864–868 (2022).
36. R. Wang, J. Chen, K. Gao, G. W. Wei, Vaccine-escape and fast-growing mutations in the United Kingdom, the United States, Singapore, Spain, India, and other COVID-19-devastated countries. *Genomics* **113**, 2158–2170 (2021).
37. J. H. Tian *et al.*, SARS-CoV-2 spike glycoprotein vaccine candidate NVX-CoV2373 immunogenicity in baboons and protection in mice. *Nat. Commun.* **12**, 372 (2021).
38. F. P. Polack *et al.*, Safety and efficacy of the BNT162b2 mRNA covid-19 vaccine. *N. Engl. J. Med.* **383**, 2603–2615 (2020).
39. L. R. Baden *et al.*, Efficacy and safety of the mRNA-1273 SARS-CoV-2 vaccine. *N. Engl. J. Med.* **384**, 403–416 (2021).
40. D. Hillus *et al.*, Safety, reactogenicity, and immunogenicity of homologous and heterologous prime-boost immunisation with ChAdOx1-nCoV19 and BNT162b2: a prospective cohort study. *Lancet Respir. Med.* **9**, 1255–1265 (2021).
41. D. S. Khoury *et al.*, Neutralizing antibody levels are highly predictive of immune protection from symptomatic SARS-CoV-2 infection. *Nat. Med.* **27**, 1205–1211 (2021).
42. M. F. Bachmann *et al.*, The influence of antigen organization on B cell responsiveness. *Science* **262**, 1448–1451 (1993).
43. K. M. Wuertz *et al.*, A SARS-CoV-2 spike ferritin nanoparticle vaccine protects hamsters against Alpha and Beta virus variant challenge. *NPJ Vaccines* **6**, 129 (2021).
44. B. Nguyen, N. H. Tolia, Protein-based antigen presentation platforms for nanoparticle vaccines. *NPJ Vaccines* **6**, 70 (2021).
45. M. F. Bachmann, G. T. Jennings, Vaccine delivery: A matter of size, geometry, kinetics and molecular patterns. *Nat. Rev. Immunol.* **10**, 787–796 (2010).
46. US Department of Health & Services, FDA. Drug products, including biological products, that contain nanomaterials–Guidance for industry (2022).
47. A. Jegerlehner *et al.*, Regulation of IgG antibody responses by epitope density and CD21-mediated costimulation. *Eur. J. Immunol.* **32**, 3305–3314 (2002).
48. P. Emsley, K. Cowtan, Coot: Model-building tools for molecular graphics. *Acta Cryst.* **D60**, 2126–2132 (2004).
49. Y. J. Kim *et al.*, The impact on infectivity and neutralization efficiency of SARS-CoV-2 lineage B.1.351 pseudovirus. *Viruses* **13**, 633 (2021).